PAPER

Passivation efficacy study of Al_2O_3 dielectric on self-catalyzed molecular beam epitaxially grown $GaAs_{1-x}Sb_x$ nanowires

To cite this article: Mehul Parakh et al 2022 Nanotechnology 33 315602

View the article online for updates and enhancements.

You may also like

- Nanocontact resistance and structural disorder induced resistivity variation in metallic metal-oxide nanowires Y F Lin, Z Y Wu, K C Lin et al.
- Synthesis and Characterization of Pt with Transition Metal Alloy Catalyst for Polymer Electrolyte Fuel Cell Application Masato Saikawa, Md Mijanur Rahman, Ryo Furukawa et al.
- <u>Transformation of Bulk Alloys to Inorganic</u>
 Nanowires
 Alexandre Magasinksi



IOP ebooks™

Bringing together innovative digital publishing with leading authors from the global scientific community.

Start exploring the collection-download the first chapter of every title for free.

IOP Publishing Nanotechnology

Nanotechnology 33 (2022) 315602 (9pp)

https://doi.org/10.1088/1361-6528/ac69f8

Passivation efficacy study of Al_2O_3 dielectric on self-catalyzed molecular beam epitaxially grown $GaAs_{1-x}Sb_x$ nanowires

Mehul Parakh^{1,3}, Priyanka Ramaswamy^{2,3}, Shisir Devkota¹, Hirandeep Kuchoor¹, Kendall Dawkins¹ and Shanthi Iyer¹

E-mail: iyer@ncat.edu

Received 22 January 2022, revised 6 April 2022 Accepted for publication 22 April 2022 Published 11 May 2022



Abstract

This work evaluates the passivation efficacy of thermal atomic layer deposited (ALD) Al₂O₃ dielectric layer on self-catalyzed GaAs_{1-x}Sb_x nanowires (NWs) grown using molecular beam epitaxy. A detailed assessment of surface chemical composition and optical properties of Al₂O₃ passivated NWs with and without prior sulfur treatment were studied and compared to as-grown samples using x-ray photoelectron spectroscopy (XPS), Raman spectroscopy, and low-temperature photoluminescence (PL) spectroscopy. The XPS measurements reveal that prior sulfur treatment followed by Al₂O₃ ALD deposition abates III–V native oxides from the NW surface. However, the degradation in 4K-PL intensity by an order of magnitude observed for NWs with Al₂O₃ shell layer compared to the as-grown NWs, irrespective of prior sulfur treatment, suggests the formation of defect states at the NW/dielectric interface contributing to non-radiative recombination centers. This is corroborated by the Raman spectral broadening of LO and TO Raman modes, increased background scattering, and redshift observed for Al₂O₃ deposited NWs relative to the as-grown. Thus, our work seems to indicate the unsuitability of ALD deposited Al₂O₃ as a passivation layer for GaAsSb NWs.

Supplementary material for this article is available online

Keywords: atomic layer deposition (ALD), Al_2O_3 passivation, $GaAs_{1-x}Sb_x$ nanowires (NWs), molecular beam epitaxy (MBE), dielectric/III–V nanowire interface

1

Introduction

III–V semiconductor nanowires (NWs) are being pursued as a potential candidate for next-generation electro-optical devices. They offer unique and superior properties stemming from their anisotropic geometry compared to their bulk counterparts [1–3]. The self-catalyzed vapor–liquid–solid growth mechanism of these nanowires enables high phase purity growth with excellent homogeneity amongst NW ensembles [4], thus eliminating foreign contamination and induced

defects arising from metal-catalyzed growth that has been commonly used until recently. However, the presence of a high density of surface states arising due to the anisotropic NW geometry is detrimental to the efficiency, sensitivity, and speed of these self-catalyzed III–V NW devices [5]. The severity of surface state formation depends on the un-passivated dangling bonds arising from the sharp termination of material growth radially and native oxide formation. These can act as non-radiative recombination centers or surface charge traps, thereby increasing surface scattering leading to decreased carrier mobility and increased density of electronic states within the bandgap, causing Fermi level pinning at the

¹ Nanoengineering, Joint School of Nanoscience and Nanoengineering, North Carolina A&T State University, Greensboro NC, 27401, United States of America

² Department of Electrical and Computer Engineering, North Carolina A&T State University, Greensboro NC, 27411, United States of America

³ Mehul Parakh and Priyanka Ramaswamy share the joint first authorship.

surface [6]. It is known [7] that the Fermi level pinning creates a depletion region on the surface, which can extend throughout the NW volume, rendering it entirely insulating or non-conducting, thereby hindering the use of NWs for practical applications. Hence, to reduce the effect of surface states, different passivation schemes have been investigated, namely ex situ treatment using wet chemical processes involving sulfur [8], hydrazine-sulfide [9], and in situ treatment involving shell growths of AlGaAs [10, 11], or InGaP [12]. Among these, treatment with sulfur and hydrazine-sulfide for long-term passivation is limited, inconvenient because of tedious chemical process control, and in the latter case hazardous due to its combustible and toxic nature. In contrast, the constraint of in situ passivation is the difficulty in obtaining shell growth uniformity for high-aspect-ratio NWs due to the shadowing effect [13]. Therefore, there is a need to explore suitable passivation techniques for III-V NWs that can provide long-term stability against any ambient variation and process convenient.

Recently, high k-dielectric materials such as Al₂O₃ and HfO₂ are emerging as promising candidates for III–V planar device passivation [14]. Among these, atomic layer deposited (ALD) Al₂O₃ layers has been attracting attention. This is due to the flexibility of ex situ deposition by ALD, enabling precise thickness control and unpinning of the Fermi level, owing to the inherent native-oxide cleaning property of Trimethylaluminum (TMA) precursor during the initial cycles of deposition [15, 16]. Further, low leakage current density $(10^{-8} \text{ A cm}^{-2})$ and low interfacial density $(D_{\rm it} \sim 10^{12} \, {\rm eV}^{-1})$ cm⁻²) are reported on Al₂O₃ ALD deposited III-V planar devices [17-19]. In addition, its larger bandgap compared to HfO₂ and good environmental resistance are some key advantages cited for its potential use as a passivation layer [20]. In NWs, however, there have been mixed results. Enhanced PL characteristics and suppressed surface recombination velocity of $\sim 10^3$ cm s⁻¹ were observed in In-based III-V NWs with ALD Al₂O₃ deposited passivation layers [21, 22]. In contrast, in thin GaAs NWs of 40 nm diameter, the passivation effect of the Al₂O₃ layer on the NWs was absent, as evidenced by the lack of PL emission for both asgrown and Al₂O₃ passivated NWs [23]. It was attributed to strong Fermi level pinning by large surface state density of thin NWs, leading to complete depletion.

In the last few decades, arsenide–antimonide (As–Sb) based material systems, particularly mixed-anion $GaAs_{1-x}Sb_x$ materials, are among the promising candidates for widespread device applications from photonics to electronics [24–26]. The ability of bandgap tuning by varying Sb composition in GaAsSb materials makes the system attractive for tunable bandgap lasers [27] and photodetectors [28–31] in the nearinfrared spectrum range. Despite the broad range of applications, the high surface recombination velocity and complex nature of native oxides pose a challenge in finding a suitable passivation layer, limiting their potential use in device technologies.

This report on the *ex situ* passivation of MBE-grown Gabased As–Sb NWs was motivated by the simplicity of Al₂O₃ *ex situ* deposition and its success in the past oxide passivation

studies on III-V thin films and NWs, including mixed As-Sb system [21–23, 32]. This work examines the efficacy of the Al₂O₃ passivation layer deposited by thermal ALD technique on self-catalyzed ensemble GaAsSb NWs using surface and optical characterization tools, namely XPS, PL spectroscopy, and Raman spectroscopy. A systematic 4K-PL study carried on Al₂O₃ passivated NW samples observed a severe optical degradation compared to as-grown samples. XPS analysis indicated that the precleaning with sulfur treatment before the deposition of the Al₂O₃ shell layer effectively removed III-V native oxides formed on the NW surface, thereby eliminating their role in optical degradation of the Al₂O₃ passivated NW samples. From Raman analysis, increased background scattering, spectral broadening of LO and TO Raman modes, and enhanced redshift compared to the as-grown NWs suggest increased density of point defects due to complex NW/dielectric interface reconstruction. These act as non-radiative recombination centers and can be the main contributors towards the optical degradation of GaAsSb NWs on Al₂O₃ shell layer deposition.

Results and discussions

The growth rate of Al₂O₃ deposition by thermal ALD was initially calibrated using 90 cycles of trimethylaluminum (TMA) and water vapor precursors on GaAs (100) substrates, which has undergone similar substrate preparations as SAO NWs mentioned in the Methods section. Statistical wafer grid scans with 49 average points using spectroscopic ellipsometry on Al₂O₃ deposited GaAs wafer was performed for refractive index versus thickness measurements as shown in Supplementary (figure S1 (available online at stacks.iop.org/ NANO/33/315602/mmedia)), which yielded Al₂O₃ oxide layer thickness of $\sim 9.6 \pm 0.5$ nm. This corresponds to an average growth rate of $\sim 1.01-1.12$ A⁰/cycle and refractive index $(n_{\rm f}) \sim 1.65 \pm 0.1$, as ascertained using a 633 nm wavelength light source. The slight deviation of the observed refractive index from ~1.63 corresponding to the stoichiometric Al₂O₃ layer grown on GaAs (100) substrate can be correlated to the complex interface layer formed between the dielectric and the GaAs surface due to the spurious oxidation effect of GaAs [33]. III-V semiconductors, in general, are known for their high surface reactivity, posing a challenge for ideal interface formation during the subsequent device processing steps. Hence, chemical passivation by sulfur was employed before Al₂O₃ ALD deposition on self-catalyzed GaAsSb NWs to minimize this effect. This study used Al₂O₃ deposition thickness of \sim 3–4 nm based on the past passivation reports [16, 18, 32].

Scanning electron microscopy

The SEM images of R, AO, and SAO samples, as shown in figures 1(a)–(c), reveal high-density vertical NWs with an average length (measured for around 50 NWs) of \sim 0.7 \pm 0.2 μ m. From the inset of SEM images, the observed

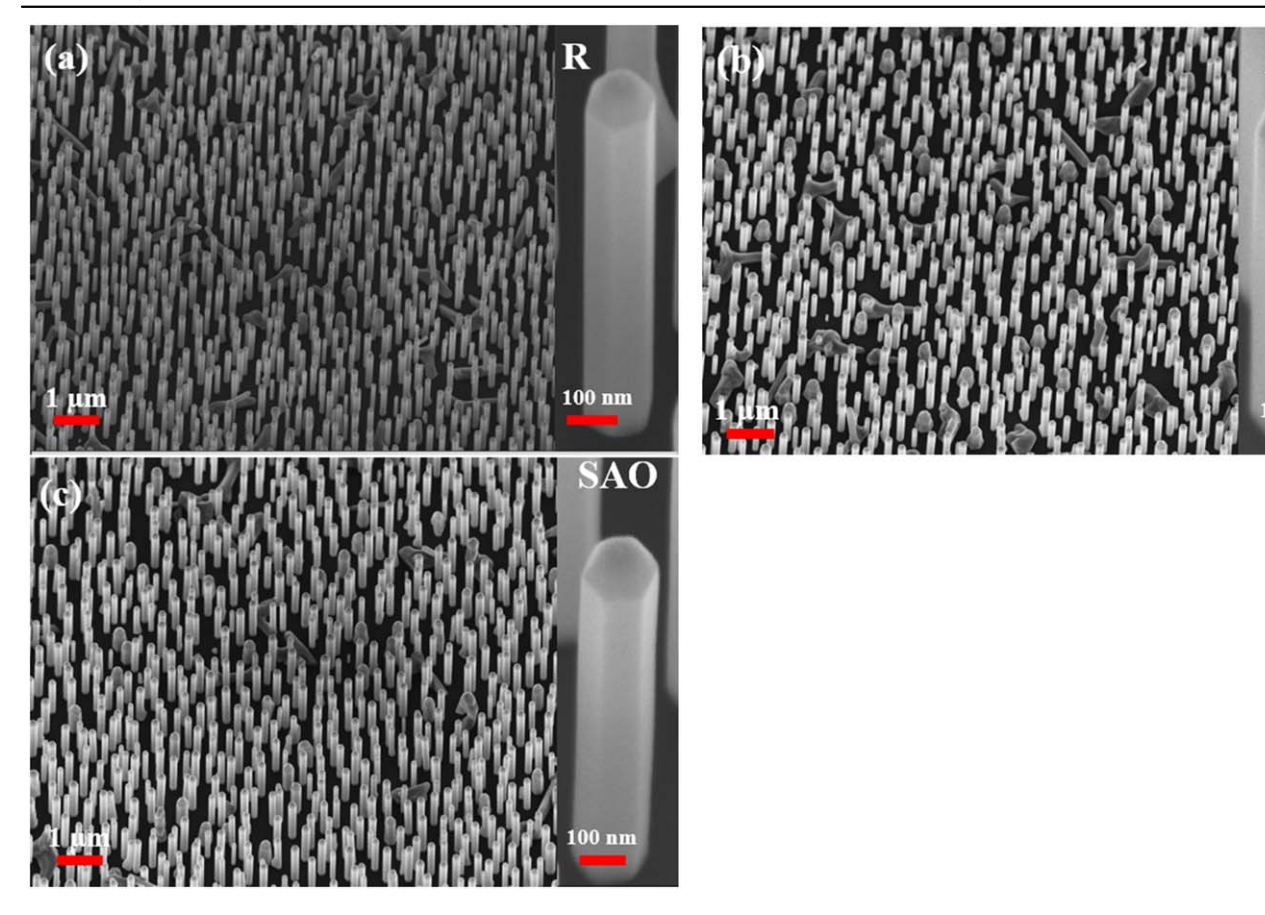


Figure 1. SEM images of self-catalyzed GaAsSb NW samples: (a) R, (b) AO, and (c) SAO (inset: SEM images of corresponding SNW).

average single nanowire (SNW) diameter for the R sample was $\sim \! 140 \pm 5$ nm, AO sample, and the SAO sample were $\sim \! 148 \pm 5$ nm, yielding a uniform Al $_2$ O $_3$ layer deposition thickness of $\sim \! 3.5 \pm 0.5$ nm on the NW surface.

It is to be noted that all these samples are based on the growth conditions published elsewhere [28, 34], where the crystal structure was confirmed to exhibit zincblende structure with an Sb composition of 7%, as determined from the scanning transmission electron microscope and energy-dispersive x-ray spectroscopy, respectively.

X-ray photoelectron spectroscopy

XPS spectra of binding energy between 0 and 150 eV of self-catalyzed GaAsSb NW samples R, AO, and SAO are shown in figure 2. The peaks of O 2s, Al 2p, and Al 2s at 23.3 eV, 74.6 eV, and 118.9 eV, respectively, present only in AO and SAO NW samples attest to the formation of the Al₂O₃ passivation layer on the surface [35].

The core-level spectra of Ga 3d and As 3d of as-grown R sample are depicted in figure 3, whereas figure 4 represents Al 2s, O 1s, Ga 3d, and As 3d spectra of AO and SAO samples. The peaks observed at 21 eV and 44.5 eV (figures 3(a) and (b)) are assigned to Ga and As complex native oxide-related peaks, respectively [32]. The atomic ratio of O/Al is 1.7 and 1.3 for AO (figures 4(a) and (b)) and SAO (figures 4(c) and (d)) samples, respectively. The appearance of Ga–O

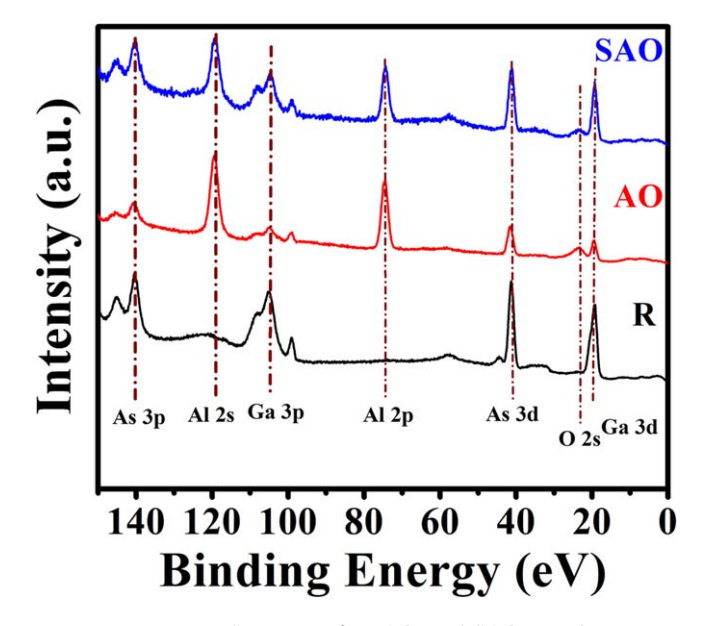


Figure 2. XPS spectra of R, AO, and SAO samples.

(figure 4(e)) only in the AO sample corroborates the observed increase in O: Al stoichiometry in this sample. It is speculated that the interdiffusion of oxygen during ALD deposition from native oxides to the Al_2O_3 passivation layer has contributed to the higher O/Al ratio in the AO sample. The absence of satellite peaks (figures 4(a)–(d)) rules out the formation of any other sub-oxide species of Al during the ALD deposition of

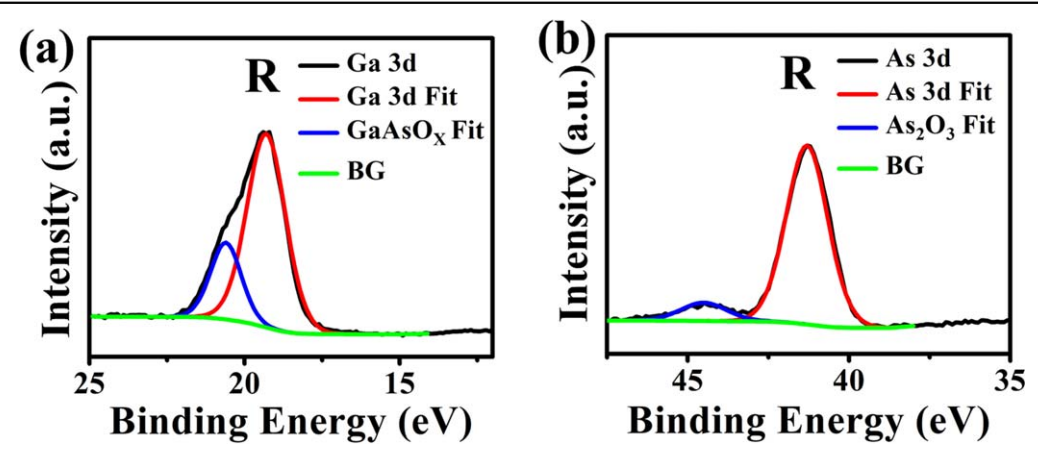


Figure 3. XPS spectra of Ga 3d and As 3d of R sample.

the Al_2O_3 passivation layer on NWs [33]. A lack of As–O peak (figures 4(f) and (h)) on Al_2O_3 deposited NWs in both non-sulfur and sulfur treated samples can be viewed as evidence of the self-cleaning process of TMA [16]. Therefore, sulfur treatment before the deposition of 3 nm of the Al_2O_3 passivation layer effectively removes the native oxides of Ga in NW samples. Further, Sb 3d signal was not registered in any of the GaAsSb NWs, which we attribute to a strong O 1s signal due to the overlapping binding energies of O 1s and Sb 3d peaks [36]. The other contributing factors could also arise from radial variation in Sb composition due to the As–Sb exchange mechanism at the NW surface [37], manifesting in Sb composition reduction at the surface as the XPS probing depth is $\Box 10$ nm.

Low-temperature photoluminescence spectroscopy (4K-PL)

Next, the optical properties of the passivation effects of sulfur treatment and Al_2O_3 deposition on self-catalyzed Te-doped GaAsSb NWs compared to as-grown were assessed by 4K-PL spectroscopy characteristics of samples R with AO and SAO shown in figure 5.

The lack of sharp low energy onset in all the samples suggests the presence of defects attributed to acceptor vacancies in GaAsSb NWs. A drastic reduction in 4K-PL intensity by a factor of $\sim \! 10$ accompanied by increased FWHM was observed for AO and SAO samples, indicating the dominance of non-radiative recombination centers. Also, a small blue shift of $15{-}18$ meV in the PL peak energy for these samples is attributed to the strain-induced due to the Al₂O₃ layer lattice mismatch with the NW surface. From SEM images (figure 1), the density of the NWs is found to be nearly uniform, hence ruling out the effect of variation in the NW density within the sample.

Recently, Ren *et al* [21] hypothesized that Al–O participates in interfacial bonding by substituting sulfur terminated bonds during Al₂O₃ deposition on InAsSb NWs. These probably elucidate why AO and SAO samples in this study observe similar PL results, with no observable effect of prior

sulfur treatment on NW passivation. Dhaka et al [23] has already shown a lack of improvement of the GaAs NW optical quality with the Al₂O₃ passivation layer. However, it is essential to note that no PL emission was observed in their both as-grown and Al₂O₃ deposited GaAs NWs. They attributed this effect to the thin diameter of as-grown GaAs NWs (~40 nm diameter) pinning the Fermi level. However, as GaAsSb NWs in this work are much thicker ~140 nm in diameter, PL deterioration due to the Fermi level pinning effect can be ruled out. Therefore, the reason for deterioration is different and probably more complex. Further, similar degradation in optical PL intensity has been observed for InP NWs after ALD deposition of HfO₂ [38]. It is to be noted that though data on only three representative samples are shown here, due to the conflicting reports of Al₂O₃ passivation effects on III-V NWs [21-23], the PL measurements were carried out on three sets of samples from different growth runs of both intrinsic and Te-doped NWs to ensure the reproducibility of observed results (shown in supplementary figure S2).

The optical degradation of NWs after Al₂O₃ deposition, irrespective of sulfur treatment or lack of it, indicates the presence of defect states contributing to non-radiative recombination centers. These defect states can be speculated to arise from (i) gap states or antibonding levels created on burying of As and Sb group V dimers formed during surface reconstruction under the Al₂O₃ layer, and/or (ii) complex interface reconstruction at the NW/dielectric interface due to lower symmetry of the surface than the bulk and presence of different surfaces [39, 40]. This complex NW/dielectric interface reconstruction can give rise to the large density of point defects because well-ordered interface layers are known to exhibit fewer point defects due to lower interface state density [41]. Further, the different surfaces of the onedimensional configuration of the NWs may promote complex NW/dielectric interface reconstruction, enhancing interface state density. GaAsSb NWs are rich in exhibiting welldefined facets, as is the case in our grown NWs as well (SNW images in figures 1(a) and (b)). Besides these, the contribution from defect states on the semiconductor side, the presence of trap states, and native point defects in the Al₂O₃ layer itself

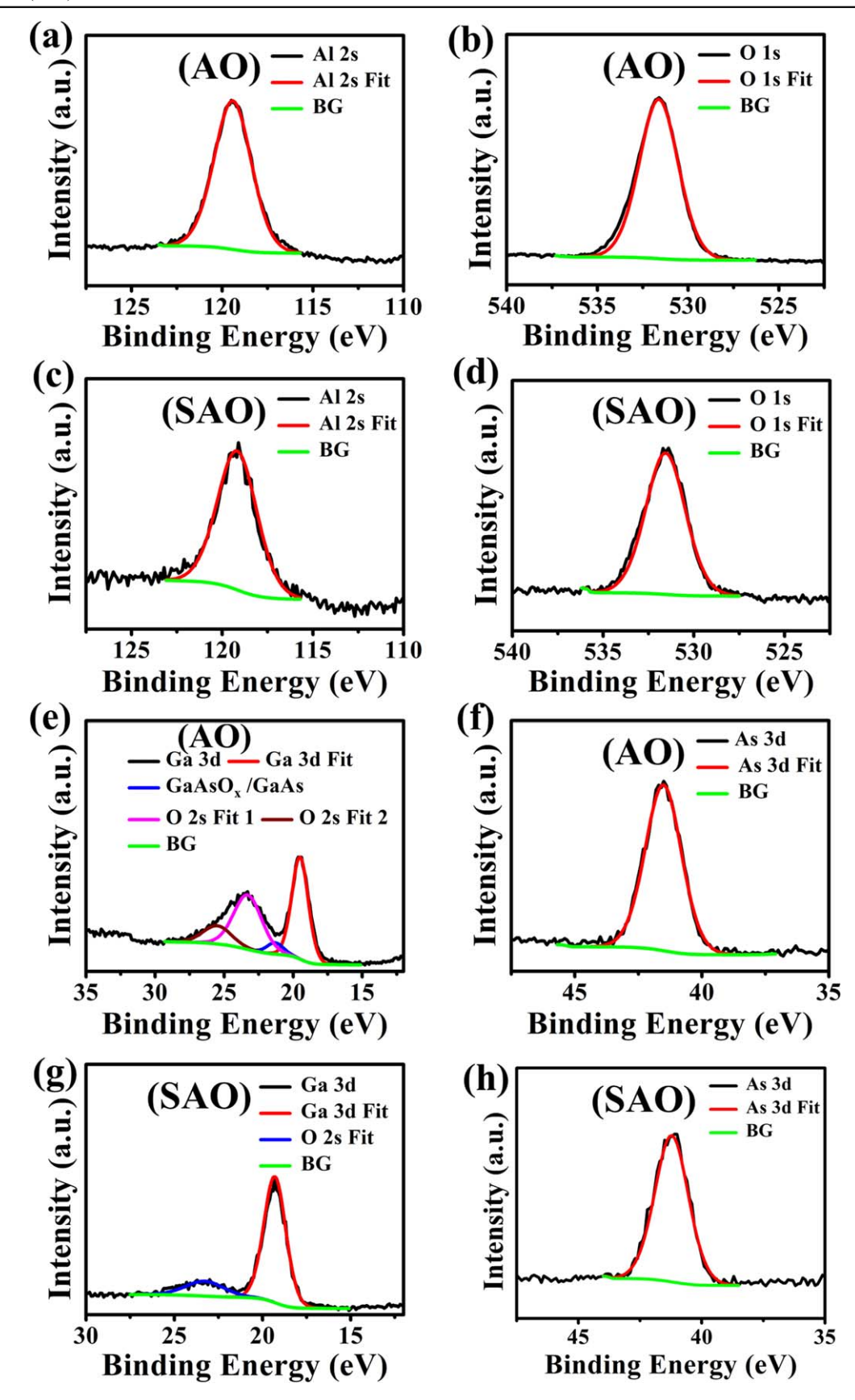


Figure 4. XPS spectra for (a), (c) Al 2s and (b), (d) O 1s of (1st row) AO and (2nd row) SAO NW samples, respectively. XPS spectra for (e), (g) Ga 3d and (f), (h) As 3d of (3rd row) AO and (4th row) SAO NW samples, respectively.

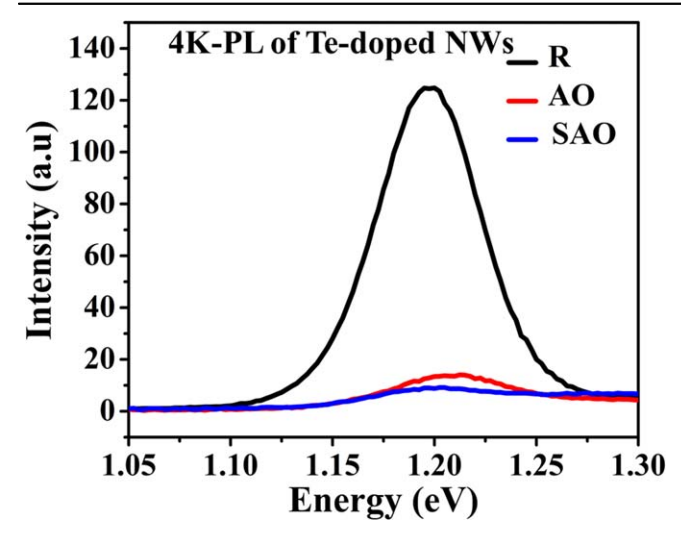


Figure 5. 4K-PL comparison of Te-doped GaAsSb: R, AO, and SAO samples.

cannot be ruled out [42, 43]. Generally, higher bandgap (bandgap higher than incoming radiation) passivation layers are preferred due to their transparency to incoming radiation. Al_2O_3 being a high-bandgap material $\sim 7~eV$ with a lower refractive index than GaAsSb, promotes waveguiding effect in the NWs. Therefore, the contribution from absorption and scattering in the oxide can be neglected.

Our observations are contrary to those observed in InAsSb NWs [21] and InP NWs [22], where Al₂O₃ layer passivation resulted in enhanced PL intensity. This can be attributed to a higher atomic radius of In when compared to Ga, thereby promoting long-range ordering at the interface [41]. This can increase the number of chemical bonds formed with the dielectric, providing better surface ordering, resulting in comparatively less defect state density. Hence, both factors contribute to an overall reduction in the interface state density [44] in In-based compounds. Thus, the Al₂O₃ passivation layer for GaAsSb NWs is inefficient due to the combination of NW anisotropy involving different facets/surface steps and a small atomic radius of Ga atoms promoting short-range surface ordering, thereby creating complex NW/dielectric reconstruction, resulting in a high density of defect states when compared to planar III-V's and In-based III-V NWs. However, 4K-PL spectra of R sample exhibited increased PL intensity with in situ grown AlGaAs passivating shell (shown in supplementary figure S3) [45, 46], thus demonstrating why AlGaAs is commonly preferred in situ passivation layer for Ga-based III-V NWs.

Raman spectroscopy

Raman spectroscopy was carried out as the shape of the Raman peak and spectral shift direction can reveal further insight into the nature of the defects. It has been reported that point defects induce spectral shift but do not give rise to asymmetry and vice versa for planar defects [31, 47–49]. Figure 6 shows the RT Raman spectra comparison of R, AO,

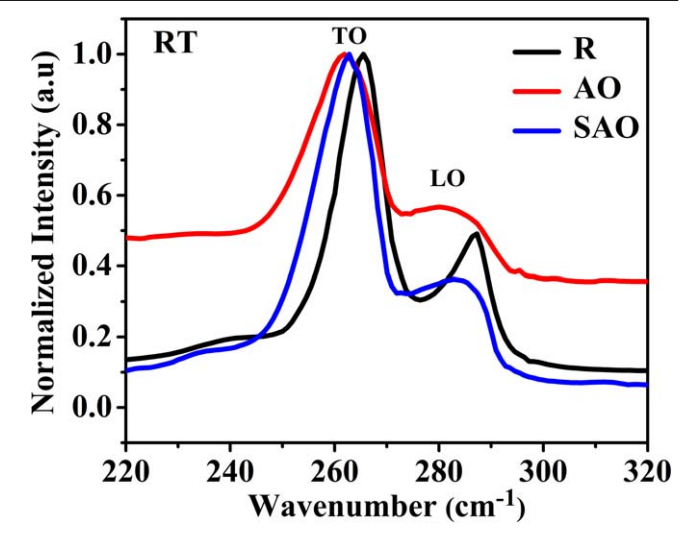


Figure 6. Normalized RT Raman spectra comparison of R, AO, and SAO samples.

and SAO samples. GaAs TO and LO vibrational mode peaks at 265 cm⁻¹ and 285 cm⁻¹, respectively, were observed in the R sample [31]. The AO sample demonstrates a significant redshift of 3.5 cm⁻¹ and a broad LO and TO mode spectra relative to the R sample, attributed to the induced strain on the NW surface during oxide deposition and phonon localization at the defects [25, 31, 49–51]. Further, the broad asymmetry is consistent with our conjecture of defect enhancement arising from complex NW/dielectric interface reconstruction, as explained in the PL section. Similar features are observed in the SAO sample with reduced peak broadness, suppressed background scattering intensity, and a comparatively smaller redshift of 2.5 cm⁻¹. These are possibly related to the more effective removal of III-V native oxides formed on the NW surface by sulfur treatment in SAO samples compared to AO, as observed from XPS measurements, aiding in reducing defects [29]. A nearly symmetric LO and TO peaks and redshifts in both the AO and SAO samples indicate the nature of defects being predominantly point defects, as the symmetric line shape of Raman suggest point defects while asymmetric line shape shows the presence of planar defects [25, 51, 52]. Raman characterization thus further strengthens the conjecture of defect creation at NW/dielectric interface on Al₂O₃ deposition and ascertains the positive effect of presulfur treatment on NWs before oxide deposition. It is to be noted that an in-depth structural analysis is required to further strengthen these claims.

Conclusion

The effect of sulfur treatment and Al_2O_3 passivation using thermal ALD $ex\ situ$ deposition on self-catalyzed GaAsSb NWs using XPS, PL spectroscopy, and Raman spectroscopy were successfully studied. The 4K-PL spectra revealed a significant drop in PL intensity ($\sim \! 10 \!$ -fold) for Al_2O_3 passivated NWs compared to as-grown irrespective of prior sulfur treatment. The XPS spectral analysis indicated that

Table 1. Sample preparation for as-grown GaAsSb NWs.

Nomenclature	NWs samples	Preclean & wet passivation	Al ₂ O ₃ ALD cycles
R	GaAsSb core	_	_
AO	GaAsSb core	_	30
SAO	GaAsSb core	Yes	30

precleaning with sulfur treatment before Al₂O₃ ALD deposition effectively removed III-V native oxides formed on the NW surface, thus ruling out the effect of native oxides on optical degradation. Further, the Raman characterization observed significant redshifts, peak broadening, and asymmetry for Al₂O₃ passivated NWs when compared to as-grown NWs, suggesting the presence of point defects on Al₂O₃ ALD deposition. Hence, the 4K-PL optical degradation observed in both sulfur treated and untreated Al₂O₃ passivated NWs samples suggests non-radiative recombination centers arising from complex NW/dielectric interface formation to be the main contributing factor. Reporting of similar PL degradation in GaAs NWs, while enhanced PL intensity in In-based NWs [23] allows us to speculate that non-radiative recombination centers arising from the Al₂O₃/NW interface states are peculiar to Ga-based III-V NWs only, and surface faceting in GaAsSb NWs may also enhance this contribution. Thus, ALD deposited Al₂O₃ layer is not a good choice for the passivation layer for GaAsSb NWs.

Materials and methods

Material synthesis

The growth of Ga-catalyzed axial GaAsSb NWs on Si (111) substrate was carried out via a vapor–liquid–solid growth mechanism using EPI 930 solid source MBE system. The Sb₂ and As₄ flux were provided by valved cracker sources operating at 900 °C and 600 °C, respectively. Axial n-GaAsSb NWs (Sb flux $\sim\!17\%$ and GaTe source temperature $\sim\!530$ °C) with group V/III flux ratio $\sim\!5.4$ at a substrate temperature of 620 °C was preset to yield a nominal growth rate of 1.1 nm s $^{-1}$. Ga-catalyzed epitaxial growth was initiated with Ga opening a few seconds before opening the group V fluxes. Later, ex situ Al₂O₃ passivation layer thickness of $\sim\!3$ –4 nm at 200 °C was deposited on NW samples using trimethylaluminum (TMA) and water vapor as precursors in Savannah S200 thermal ALD system, operating at 0.5 mTorr base pressure.

Material characterization

Surface analysis was performed on a Thermo ESCALAB 250 Xi with the base chamber pressure of 10^{-10} Torr, equipped with a monochromated Al K α x-rays source of $h\nu=1486.6\,eV$ for XPS measurements, at room temperature. Micro-PL spectroscopy system at 4 K temperature was used to measure the optical characteristics of NWs, which employ

a 633 nm He-Ne laser as the source excitation, 0.32 m double grating monochromator, and InGaAs detector with conventional lock-in techniques. A closed-cycle optical cryostat from Montana cryostation was used for cooling the samples. Raman spectroscopy was performed in a Horiba Jobin Yvon ARAMIS Raman microscope with a He-Ne laser of 633 nm as the excitation source at room temperature. It is to be noted that all the measurements were performed on the NW ensemble. We have studied three sets each of n-type doped and intrinsic NW samples, where each set corresponds to all three R, AO, and SAO type samples. The ensemble NW sample was cut into four quadrants. Each quadrant was used for different characterization; hence the density variation is minimum among these different quadrants from the same ensemble NW sample. Further, for PL analysis, multiple spots (five on one quadrant) were performed for uniformity in the observed peak position and intensity.

Methods

In this work, three axial self-catalyzed GaAsSb NW samples were grown to investigate the effect of preclean and surface passivation technique in conjunction with *ex situ* thermal ALD deposited Al₂O₃ passivation layer. They include three types of GaAsSb NW samples. The two grown samples are (R) as-grown reference NW and (AO) as-grown with *ex situ* Al₂O₃ passivation layer. The third sample, referred to as SAO, is as-grown GaAsSb NWs submerged initially in HCl aqueous solution (for native oxide removal) followed by 5 min in 1:10 (NH₄)₂S/H₂O diluted solution (for sulfur passivation), immediately blown dried by nitrogen (without rinsing with deionized water to minimize any loss of sulfur from the surface) and quickly transferred to a thermal ALD system for depositing Al₂O₃ passivation layer. All the samples used in this study are listed below in table 1.

Acknowledgments

This work is primarily based upon research supported by the Air Force Office of Scientific Research (AFOSR) under grant number W911NF1910002. The National Science Foundation (NSF) also funded a part of this work under grant# 1832117. This work was performed at the Joint School of Nanoscience and Nanoengineering, a member of the Southeastern Nanotechnology Infrastructure Corridor (SENIC) and National Nanotechnology Coordinated Infrastructure (NNCI), which is supported by the National Science Foundation (ECCS-1542174).

Data availability statement

All data that support the findings of this study are included within the article (and any supplementary files).

ORCID iDs

Mehul Parakh https://orcid.org/0000-0003-0014-7443 Priyanka Ramaswamy https://orcid.org/0000-0002-7692-3907

Shanthi Iyer https://orcid.org/0000-0002-8163-9943

References

- [1] LaPierre R R et al 2017 A review of III–V nanowire infrared photodetectors and sensors J. Phys. D: Appl. Phys. 50 123001
- [2] Nalamati S et al 2019 A study of GaAs_{1-x}Sb_x axial nanowires grown on monolayer graphene by Ga-assisted molecular beam epitaxy for flexible near-infrared photodetectors ACS Appl. Nano Mater. 2 4528–37
- [3] Ramaswamy P et al 2021 Be-Doping Assessment in Self-Catalyzed MBE Grown GaAs Nanowires. in CLEO: Science and Innovations (San Jose, California United States: Optical Society of America) pp SW2F-7
- [4] Tersoff J 2015 Stable self-catalyzed growth of III–V nanowires Nano Lett. 15 6609–13
- [5] Fukata N and Rurali R 2020 Fundamental Properties of Semiconductor Nanowires (Berlin: Springer) (https://doi. org/10.1007/978-981-15-9050-4)
- [6] Demichel O et al 2010 Impact of surfaces on the optical properties of GaAs nanowires Appl. Phys. Lett. 97 201907
- [7] Simpkins B S *et al* 2008 Surface depletion effects in semiconducting nanowires *J. Appl. Phys.* **103** 104313
- [8] Tajik N et al 2011 Sulfur passivation and contact methods for GaAs nanowire solar cells Nanotechnology 22 225402
- [9] Alekseev P A *et al* 2015 Nitride surface passivation of GaAs nanowires: impact on surface state density *Nano Lett.* **15**
- [10] Dai X et al 2014 GaAs/AlGaAs nanowire photodetector Nano Lett. 14 2688–93
- [11] Parakh M et al 2020 Space charge limited conduction mechanism in GaAsSb nanowires and the effect of in situ annealing in ultra-high vacuum Nanotechnology 31 025205
- [12] Skold N et al 2005 Growth and optical properties of strained GaAs-GaxIn 1-x P core–shell nanowires Nano Lett. 5 1943–7
- [13] André Y et al 2020 Optical and structural analysis of ultra-long GaAs nanowires after nitrogen-plasma passivation Nano Express 1 (2) 020019
- [14] Timm R et al 2011 Interface composition of atomic layer deposited HfO₂ and Al₂O₃ thin films on InAs studied by x-ray photoemission spectroscopy Microelectron. Eng. 88 1091–4
- [15] Driad R et al 2011 Atomic layer deposition of aluminum oxide for surface passivation of InGaAs/InP heterojunction bipolar transistors J. Electrochem. Soc. 158 H1279
- [16] Milojevic M et al 2008 Half-cycle atomic layer deposition reaction studies of Al₂O₃ on (NH4)2S passivated GaAs(100) surfaces Appl. Phys. Lett. 93 252905
- [17] Huang M L et al 2005 Surface passivation of III–V compound semiconductors using atomic-layer-deposition-grown Al₂O₃ Appl. Phys. Lett. 87 252104

- [18] Yi X, Hung-Chun L and Ye P D 2007 Simplified surface preparation for GaAs passivation using atomic layerdeposited high- \$\kappa\$ dielectrics IEEE Trans. Electron Devices 54 1811-7
- [19] Luo L-B et al 2015 A graphene/GaAs near-infrared photodetector enabled by interfacial passivation with fast response and high sensitivity J. Mater. Chem. C 3 4723–8
- [20] Rahman M M et al 2019 Characterization of Al incorporation into HfO2 dielectric by atomic layer deposition Micromachines (Basel) 10 361
- [21] Ren D et al 2019 Room-temperature midwavelength infrared InAsSb nanowire photodetector arrays with Al₂O₃ passivation Nano Lett. 19 2793–802
- [22] Black L E et al 2017 Effective surface passivation of InP nanowires by atomic-layer-deposited Al₂O₃ with POx interlayer Nano Lett. 17 6287–94
- [23] Dhaka V et al 2016 Protective capping and surface passivation of III–V nanowires by atomic layer deposition AIP Adv. 6 015016
- [24] Xiaoguang S et al 2002 GaAsSb: a novel material for near infrared photodetectors on GaAs substrates IEEE J. Sel. Top. Quantum Electron. 8 817–22
- [25] Deshmukh P et al 2019 Molecular beam epitaxial growth of GaAsSb/GaAsSbN/GaAlAs core-multishell nanowires for near-infrared applications Nanotechnology 30 275203
- [26] Deshmukh P et al 2018 Molecular beam epitaxial growth of high quality Ga-catalyzed GaAs1–x Sb x (x > 0.8) nanowires on Si (111) with photoluminescence emission reaching 1.7 μm Semicond. Sci. Technol. 33 125007
- [27] Yu S Q et al 2007 High performance GaAsSb/GaAs quantum well lasers J. Vac. Sci. Technol. B 25 1658-63
- [28] Devkota S et al 2020 A study of n-doping in self-catalyzed GaAsSb nanowires using GaTe dopant source and ensemble nanowire near-infrared photodetector Nanotechnology 31 505203
- [29] Sharma M et al 2019 Improved performance of GaAsSb/ AlGaAs nanowire ensemble Schottky barrier based photodetector via in situ annealing Nanotechnology 30 034005
- [30] Nalamati S et al 2020 Hybrid GaAsSb/GaAs heterostructure core–shell nanowire/graphene and photodetector applications ACS Appl. Electron. Mater. 2 3109–20
- [31] Pokharel R et al 2020 Epitaxial high-yield intrinsic and Tedoped dilute nitride GaAsSbN nanowire heterostructure and ensemble photodetector application ACS Appl Electron. Mater. 2 2730–8
- [32] Liu J S, Clavel M and Hudait M K 2015 Tailoring the valence band offset of Al₂O₃ on epitaxial GaAs(1-y)Sb(y) with tunable antimony composition ACS Appl. Mater. Interfaces 7 28624–31
- [33] Sah R E et al 2013 Characterization of Al₂O₃/GaAs interfaces and thin films prepared by atomic layer deposition J. Vac. Sci. Technol. B 31 04D111
- [34] Ahmad E, Ojha S K, Kasanaboina P K, Reynolds C L, Liu Y and Iyer S 2017 Bandgap tuning in GaAs_{1 - x}Sb_x axial nanowires grown by Ga-assisted molecular beam epitaxy *Semicond. Sci. Technol.* 32 035002
- [35] Sah R E et al 2013 Characterization of Al₂O₃/GaAs interfaces and thin films prepared by atomic layer deposition J. Vac. Sci. Technol. B 31 04D111
- [36] Ramaswamy P et al 2021 A study of dopant incorporation in Te-doped GaAsSb nanowires using a combination of XPS/ UPS, and C-AFM/SKPM Sci. Rep. 11 8329
- [37] Huh J et al 2015 Rectifying single GaAsSb nanowire devices based on self-induced compositional gradients Nano Lett. 15 3709–15
- [38] Munch S *et al* 2010 Time-resolved photoluminescence investigations on HfO₂-capped InP nanowires *Nanotechnology* **21** 105711

- [39] Lin L and Robertson J 2012 Passivation of interfacial defects at III–V oxide interfaces J. Vac. Sci. Technol. B 30 04E101
- [40] Pashley M D 1989 Electron counting model and its application to island structures on molecular-beam epitaxy grown GaAs (001) and ZnSe(001) Phys. Rev. B 40 10481-7
- [41] Laukkanen P et al 2021 Passivation of III–V surfaces with crystalline oxidation Appl. Phys. Rev. 8 011309
- [42] Fleetwood D M et al 1993 Effects of oxide traps, interface traps, and 'border traps' on metal—oxide—semiconductor devices. J. Appl. Phys. 73 5058–74
- [43] Choi M, Janotti A and Van de Walle C G 2013 Native point defects and dangling bonds in α-Al₂O₃. J. Appl. Phys. 113 044501
- [44] Scarrozza M et al 2009 A first-principles study of the structural and electronic properties of III–V/thermal oxide interfaces Microelectron. Eng. 86 1747–50
- [45] Dastjerdi M H T, Boulanger J P, Kuyanov P, Aagesen M and LaPierre R R 2016 Methods of Ga droplet consumption for improved GaAs nanowire solar cell efficiency *Nanotechnology* 27 475403
- [46] Boulanger J P, Chia A C E, Wood B, Yazdi S, Kasama T, Aagesen M and LaPierre R R 2016 Characterization of a Ga-

- assisted GaAs nanowire array solar cell on Si substrate *IEEE J. Photovolt.* **6** 661–7
- [47] Ahmad E *et al* 2017 A two-step growth pathway for high Sb incorporation in GaAsSb nanowires in the telecommunication wavelength range *Sci. Rep.* 7 10111
- [48] Kasanaboina P K et al 2015 Self-catalyzed growth of dilute nitride GaAs/GaAsSbN/GaAs core–shell nanowires by molecular beam epitaxy Appl. Phys. Lett. 107 103111
- [49] Sharma M et al 2017 Growth of defect-free GaAsSbN axial nanowires via self-catalyzed molecular beam epitaxy Semicond. Sci. Technol. 32 125003
- [50] Calizo I et al 2007 Micro-Raman Spectroscopic Characterization ZnO Quantum Dots, Nanocrystals, and Nanowires. in Quantum Dots, Particles, and Nanoclusters IV (San Jose, California, United States: International Society for Optics and Photonics) (https://doi.org/10.1117/12.713648)
- [51] Kasanaboina P, Sharma M, Deshmukh P, Reynolds C L, Liu Y and Iyer S 2016 Effects of annealing on GaAs/ GaAsSbN/GaAs core-multi-shell nanowires *Nanoscale Res.* Lett. 11 1–6
- [52] Falkovsky L A 2001 Width of optical phonons: influence of defects of various geometry *Phys. Rev.* B 64 024301